

Effects of post-annealing on crystalline and transportproperties of Bi_2Te_3 thin films

Qi-Xun Guo(郭奇勋), Zhong-Xu Ren(任中旭), Yi-Ya Huang(黄意雅), Zhi-Chao Zheng(郑志超), Xue-Min Wang(王学敏), Wei He(何为), Zhen-Dong Zhu(朱振东), and Jiao Teng(滕皎)

Citation: Chin. Phys. B, 2021, 30 (**6**): 067307. DOI: 10.1088/1674-1056/abee6c

Journal homepage: http://cpb.iphy.ac.cn; http://iopscience.iop.org/cpb

What follows is a list of articles you may be interested in

Correlated insulating phases in the twisted bilayer graphene

Yuan-Da Liao(廖元达), Xiao-Yan Xu(许霄琰), Zi-Yang Meng(孟子杨), and Jian Kang(康健)

Chin. Phys. B, 2021, 30 (**1**): 017305. DOI: 10.1088/1674-1056/abcfa3

Progress on 2D topological insulators and potential applications in electronic devices

Yanhui Hou(侯延辉), Teng Zhang(张腾), Jiatao Sun(孙家涛), Liwei Liu(刘立巍), Yugui Yao(姚裕贵), Yeliang Wang(王业亮)

Chin. Phys. B, 2020, 29 (**9**): 097304. DOI: 10.1088/1674-1056/aba9c5

Electronic structure of correlated topological insulator candidate YbB_6 studied by photoemission and quantum oscillation

T Zhang(张腾), G Li(李岗), S C Sun(孙淑翠), N Qin(秦娜), L Kang(康璐), S H Yao(姚淑华), H M Weng(翁红明), S K Mo, L Li(李璐), Z K Liu(柳仲楷), L X Yang(杨乐仙), Y L Chen(陈宇林)

Chin. Phys. B, 2020, 29 (**1**): 017304. DOI: 10.1088/1674-1056/ab6206

Disorder induced phase transition in magnetic higher-order topological insulator: A machine learning study

Zixian Su(苏子贤), Yanzhuo Kang(康艳卓), Bofeng Zhang(张博峰), Zhiqiang Zhang(张智强), Hua Jiang(江华)

Chin. Phys. B, 2019, 28 (**11**): 117301. DOI: 10.1088/1674-1056/ab4582

Scanning tunneling microscopic investigation on morphology of magnetic Weyl semimetal $YbMnBi_2$

Zhen Zhu(朱朕), Dong Yan(严冬), Xiao-Ang Nie(聂晓昂), Hao-Ke Xu(徐豪科), Xu Yang(杨旭), Dan-Dan Guan(管丹丹), Shiyong Wang(王世勇), Yao-Yi Li(李耀义), Canhua Liu(刘灿华), Jun-Wei Liu(刘军伟), Hui-Xia Luo(罗惠霞), Hao Zheng(郑浩), Jin-Feng Jia(贾金锋)

Chin. Phys. B, 2019, 28 (**7**): 077302. DOI: 10.1088/1674-1056/28/7/077302

Effects of post-annealing on crystalline and transport properties of Bi_2Te_3 thin films*

Qi-Xun Guo(郭奇勋)[1,2,†], Zhong-Xu Ren(任中旭)[1,†], Yi-Ya Huang(黄意雅)[1], Zhi-Chao Zheng(郑志超)[1], Xue-Min Wang(王学敏)[2], Wei He(何为)[3], Zhen-Dong Zhu(朱振东)[4,‡], and Jiao Teng(滕蛟)[1,§]

[1] *Department of Material Physics and Chemistry, University of Science and Technology Beijing, Beijing* 100083, *China*
[2] *Collaborative Innovation Center of Advanced Steel Technology, University of Science and Technology Beijing, Beijing* 100083, *China*
[3] *Beijing National Laboratory for Condensed Matter Physics and Institute of Physics, Chinese Academy of Sciences, Beijing* 100190, *China*
[4] *National Institute of Metrology, Beijing* 100029, *China*

(Received 9 February 2021; revised manuscript received 10 March 2021; accepted manuscript online 15 March 2021)

A well-established method is highly desirable for growing topological insulator thin films with low carrier density on a wafer-level scale. Here, we present a simple, scalable method based on magnetron sputtering to obtain high-quality Bi_2Te_3 films with the carrier density down to 4.0×10^{13} cm^{-2}. In contrast to the most-used method of high substrate temperature growth, we firstly sputtered Bi_2Te_3 thin films at room temperature and then applied post-annealing. It enables the growth of highly-oriented Bi_2Te_3 thin films with larger grain size and smoother interface. The results of electrical transport show that it has a lower carrier density as well as a larger coherent length ($\sim$ 228 nm, 2 K). Our studies pave the way toward large-scale, cost-effective production of Bi_2Te_3 thin films to be integrated with other materials in wafer-level scale for electronic and spintronic applications.

Keywords: topological insulator, magnetron sputtering, post annealing, Kiessig fringes, low carrier density, weak antilocalization

PACS: 73.50.−h, 72.15.Rn, 73.20.Fz **DOI:** 10.1088/1674-1056/abee6c

Three-dimensional topological insulators (TIs) like Bi_2Te_3 have attracted considerable research attention on account of their unique energy band structure: they are insulating in the bulk and exhibit gapless metallic surface states. The nontrivial surface states of TIs have been confirmed by various methods such as angle-resolved photoemission spectroscopy experiments,[1–3] scanning tunneling microscopy/spectroscopy,[4] and transport measurements.[5] However, in most TIs, the bulk does not insulate and the Dirac point is not exposed or not close to the Fermi level, masking the topological phenomena. To utilize the unique electronic properties of the surface states, suppressing the contribution from the bulk is desirable in TIs-based electronic devices. Tremendous efforts have been made to reduce the bulk carrier density, such as using compensation doping with Sb or Se elements in Bi_2Te_3 materials,[6,7] back gate, top gate, or dual gate modulation.[8–10]

Due to the hexagonal structure of bulk Bi_2Se_3, Bi_2Te_3, and Sb_2Te_3, it is common that thin films of TIs are composed of many triangular grains and each grain has terrace-step surface morphology.[11,12] At the center of the triangular grains, the film thickness is the largest, while at the grain boundaries, the thickness is the smallest. Therefore, TI thin films may have relatively large root-mean-square surface roughness.

To grow high-quality topological insulator thin films with low roughness and suppress the bulk carriers density, several methods have been used, including molecular beam epitaxy (MBE),[13,14] pulsed laser deposition (PLD),[15,16] chemical vapor deposition (CVD),[17] and magnetron sputtering.[18] As is well known, MBE growth allows for a precise control of the growth parameters to obtain a very low density of defects. However, MBE operates in ultra-high vacuum conditions and is significantly expensive. On the other hand, magnetron sputtering is highly versatile and a well-established method for growing a variety of TIs on a large scale, which is very important for industrial applications.

In our previous work,[18] we have successfully fabricated Bi_2Te_3 thin films on 4 inches wafer by magnetron sputtering method. Here, we present a method of the heating process to obtain the high-quality Bi_2Te_3 films with low carrier density down to 4.0×10^{13} cm^{-2}. For comparison, the Bi_2Te_3 thin films were prepared by magnetron sputtering with two differ-

*Project supported by the National Natural Science Foundation of China (Grant Nos. 52072030, 52071025, and 51871018), the Beijing Outstanding Young Scientists Projects (Grant No. BJJWZYJH01201910005018), Beijing Natural Science Foundation, China (Grant No. Z180014), the Science and Technology Innovation Team Program of Foshan (Grant No. FSOAA-KJ919-4402-0087), and Beijing Laboratory of Metallic Materials and Processing for Modern Transportation.

†These authors contributed equally.
‡Corresponding author. E-mail: zd_tsu@163.com
§Corresponding author. E-mail: tengjiao@mater.ustb.edu.cn

© 2021 Chinese Physical Society and IOP Publishing Ltd

ent heating processes: one is grown at a high substrate temperature, the other is grown at room temperature then followed by post-annealing. Structure analysis using x-ray diffraction (XRD), x-ray reflectivity (XRR), and scanning electron microscope (SEM) indicates that the latter process enables the growth of highly-oriented Bi_2Te_3 thin films with larger grain size and smoother interface. Electrical transport properties show that lower carrier density and larger coherent length have been achieved in post-annealed Bi_2Te_3 thin films. Our studies pave a way for Bi_2Te_3 thin films to be integrated with magnetic multilayers and heterostructures for spintronic applications.

All of our samples were prepared by magnetron sputtering on silicon substrates (300 nm SiO_2/Si). The co-sputtering method with high purity (99.99%) Bi_2Te_3 alloying target and Te target was used to control films' composition. Direct current (DC) power source was used for Bi_2Te_3 alloying target and radio-frequency (RF) power source was used for Te target. The base pressure of the deposition chamber was below 3×10^{-7} Torr and the working argon pressure was set at 2 mTorr. Films were deposited at room temperature and the substrate temperature was kept at 240 °C. All films were capped with a 4 nm thick Al thin film. The Al thin film was naturally oxidized to form AlO_x after exposure in air and to protect the TIs layer from oxidation. The post-annealing process was performed in a vacuum of 10^{-7} Torr for 3 hours at various temperatures (200 °C, 240 °C, and 280 °C). XRD, XRR, and SEM were used to characterize the film structure. The transport properties were tested by the physical properties measurement system (PPMS) of the Quantum Design.

In Fig. 1, we present the x-ray results of the prepared samples. As described in our previous report,[18] polycrystalline Bi_2Te_3 thin films can be successfully grown at the substrate temperature of 240 °C. XRD spectrum of this sample is shown as the red curve in Fig. 1(a). We can see three peaks in this spectrum: (0 0 3), (0 0 6), and (0 0 15), showing the evidence of preferred growth with a *c*-axis orientation. We can also see that there is no obvious peak in the curve of the Bi_2Te_3 film grown at room temperature, indicating an amorphous phase. However, after annealing at 200 °C for 3 hours, the characteristic peaks of (0 0 3*n*) appeared, suggesting that the amorphous sample transformed into the crystalline phase after annealing. The full-width at half-maximum (FWHM) of (0 0 6) of the film annealed at 200 °C is about 0.6°, smaller than 0.9° of the substrate-heated sample. When the annealing temperature increased to 280 °C, the characteristic peaks still exist and the FWHM is nearly constant at 0.6°. The smaller FWHM, or sharper diffraction peaks of the annealed samples than that of the substrate heated sample means that the post-annealed Bi_2Te_3 films have a larger grain size and better crystallinity. Strong Kiessig fringes can be observed around the Bi_2Te_3 diffraction peaks, as shown in the inset of Fig. 1(a), which originate from the interference of x-ray beams reflected at the substrate–film and film–air interfaces.[19] The occurrence of these well-shaped fringes confirms a uniform and smooth surface and high crystal quality of the annealed Bi_2Te_3 films.

Figures 1(b) and 1(c) show measured XRR data (black dots) of the substrate-heated and 280 ° annealed Bi_2Te_3 films. For the substrate-heated sample (Fig. 1(c)), the XRR curve shows a monotone decrease, while for the post-annealed sample (Fig.1(d)), continuous oscillation (Kiessig fringes) can be observed. By the deepness of Kiessig fringes, we conclude that the substrate-heated Bi_2Te_3 film has a much larger roughness while the post-annealed Bi_2Te_3 film has a better interface and lower roughness, which is consistent with the results obtained from XRD. Besides, the thickness of the post-annealed Bi_2Te_3 film is determined to be 13.8 nm by using the GenX software.[20]

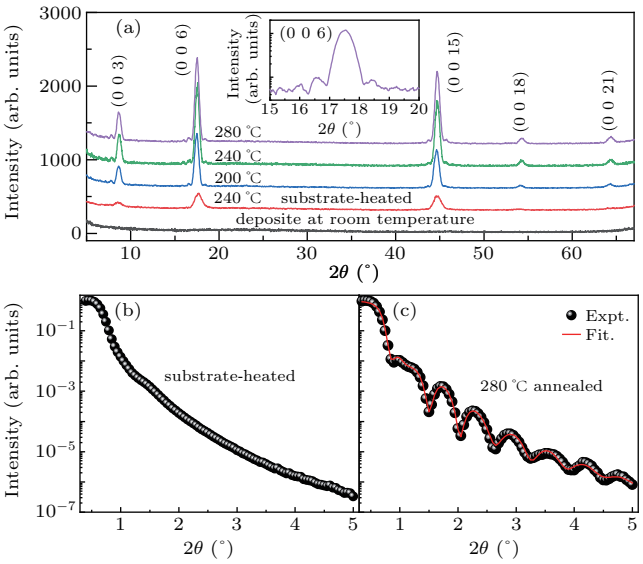


Fig. 1. XRD and XRR spectra of the Bi_2Te_3 films. (a) XRD spectra of Bi_2Te_3 films for different substrate temperatures (room temperature and 240 °C) and different annealing temperatures (200 °C, 240 °C, and 280 °C). The inset shows a fine scanned image of the BT film annealed at 280 °C between 15° and 20°. XRR spectra of the substrate-heated (b) and 280 °C annealed (c) Bi_2Te_3 films. The black dots are measured data, and the red line is the fitting curve.

Figure 2 shows SEM images of surface morphologies of Bi_2Te_3 films with different heat treatment processes. It can be seen that the surface of the as-deposited film (Fig. 2(a)) is quite flat, while the surface of the 280 ° annealed film (Fig. 2(c)) is rougher, indicating that annealing causes the growth of the grains. The film sputtered at high substrate temperature has flaky or granular morphology and is formed by grains of Bi_2Te_3 nanoplates with different sizes (Fig. 2(b)). In this image, we notice that many Bi_2Te_3 nanoplates are not parallel to the surface of the substrate, which may be responsible for the broader peaks of XRD pattern of the substrate-heated sample.

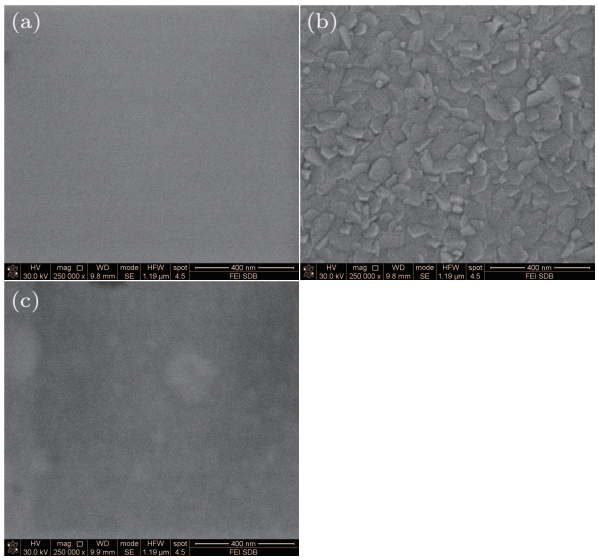


Fig. 2. SEM images for Bi_2Te_3 thin films sputtered at room temperature (a), sputtered at the substrate temperature of 240 °C (b), and sputtered at room temperature then followed by annealing at 280 °C (c).

The transport measurements were carried out in the standard Hall bar geometry. Figures 3(a) and 3(c) are the Hall curves (R_{xy}–H) of the substrate-heated and 280 °C annealed Bi_2Te_3 films, respectively. The Hall slopes of both samples at 2 K and 300 K are negative, which clearly reveals that the dominant carriers of both samples are electrons. Figures 3(b) and 3(d) show the temperature-dependent nominal carrier density of two samples estimated from R_{xy}. At 2 K, the carrier density is 13.5×10^{13} cm^{-2} for the substrate-heated sample and is 4.0×10^{13} cm^{-2} for the 280 °C annealed sample. The carrier density of the substrate-heated sample is about 3.4 times larger than that of the 280 °C annealed sample. It indicates that the carrier from bulk is largely suppressed in the 280 °C annealed Bi_2Te_3 thin films.

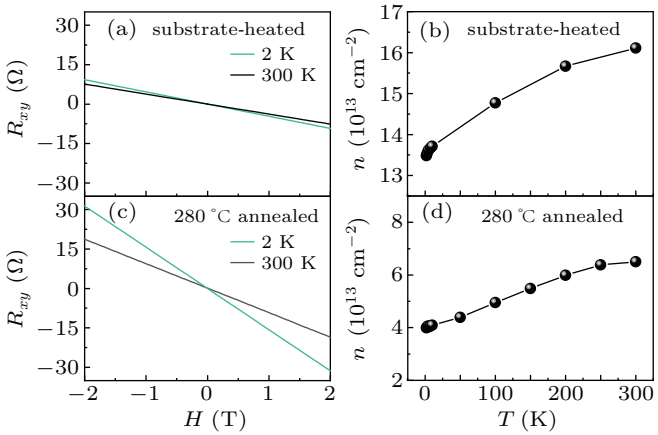


Fig. 3. Hall curves of substrate-heated (a) and 280 °C annealed (c) samples at 2 K and 300 K, respectively. Carrier density of substrate-heated (b) and 280 °C annealed (d) samples as a function of temperature.

Figure 4 shows sheet conductance σ_{xx} ($\sigma_{xx} = R_{xx}/(R_{xx}^2 + R_{xy}^2)$) of the above two Bi_2Te_3 thin films measured at various magnetic fields in the temperature range of 2 K to 10 K. A well-defined linear ln$T$ dependence of σ_{xx} is observed at low temperatures (solid lines are the linear fits). The slope of σ_{xx} is defined by $\kappa = (\pi h/e^2)\mathrm{d}\sigma_{xx}/\mathrm{d}\ln T$.[21] As shown in the inset, κ increases with increasing magnetic field and is approximately unchanged when the magnetic field ranges from 0.5 T to 2 T. The sharp increase at low magnetic fields can be attributed to the rapid suppression of the weak antilocalization (WAL) effect, and the saturated value of κ in a high field range of 0.5–2 T suggests that the effect is quenched. At the high magnetic field, the saturated κ is ascribed to the contribution of electron–electron interaction (EEI).[22,23] Interestingly, the ratio of saturated κ of these two Bi_2Te_3 thin films is very close to the ratio of the carrier density, 3.4, which suggests that the strength of EEI is proportional to the carrier density.

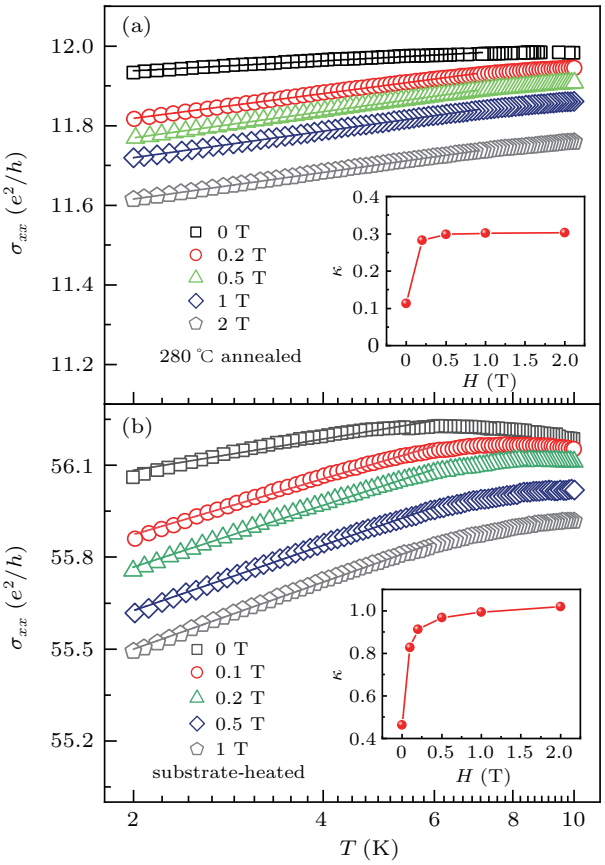


Fig. 4. Temperature dependencies of sheet conductance σ_{xx} (open symbols) recorded at different magnetic fields for (a) 280 °C annealed and (b) substrate-heated Bi_2Te_3 thin films. The straight lines are linear fits of σ_{xx} to ln$T$. Inset of each plot shows the slope $\kappa = (\pi h/e^2)\mathrm{d}\sigma_{xx}/\mathrm{d}\ln T$ as a function of magnetic field.

To further explore WAL behavior, the magnetic field dependent sheet resistance was measured at varied temperature. Figure 5(a) shows the magnetic field dependence of ΔR_{xx} of the post-annealed sample at different temperatures. The parabolic ΔR_{xx} curve at the high-temperature region (50–250 K) is ascribed to a semiclassical model that conduction electrons drift in a magnetic field and are deflected by the Lorentz force. At the low temperatures (2–10 K), the ΔR_{xx} curve is nearly linear at the high magnetic field, and a sharp dip appears near the zero magnetic field, which is a typical feature of the WAL effect. As shown in Fig. 5(b), the WAL behavior at the low magnetic field region (less than 0.5 T) can

be well fitted by Hikami–Larkin–Nagaoka (HLN) equation[24]

$$\Delta\sigma_{xx} = \sigma_{xx}(H) - \sigma_{xx}(0) = -\frac{\alpha e^2}{2\pi^2\hbar}\left[\ln\frac{\hbar}{4Bel_\varphi^2} - \psi\left(\frac{1}{2}+\frac{\hbar}{4Bel_\varphi^2}\right)\right],$$

where α is the WAL coefficient, l_φ is the phase coherence length, and $\psi(x)$ is the digamma function. It should be noted that, for the magnetic field larger than 0.5 T, the magnetoconductance is found to deviate from the HLN equation, and this is consistent with the results of κ being saturated above 0.5 T. Fitting $\Delta\sigma_{xx}$ at 2 K with the HLN equation yields $l_\varphi \sim 228$ nm and 180 nm for the 280 °C annealed and substrate-heated Bi_2Te_3 thin films, respectively. Both values are much larger than the thickness of the films (14 nm), justifying the two-dimensional WAL characteristics in our samples. The temperature dependence of l_φ of the two Bi_2Te_3 thin films is shown in Fig. 5(c).

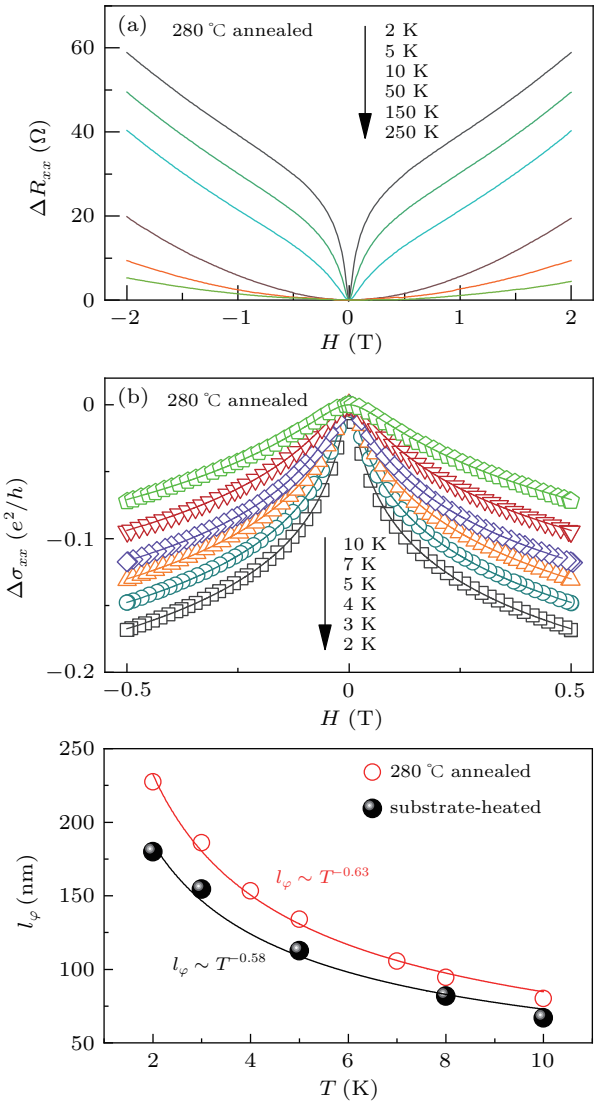


Fig. 5. (a) The ΔR_{xx} of post-annealed sample as a function of magnetic field at different temperature, $\Delta R_{xx} = R_{xx}(H) - R_{xx}(0)$. (b) Longitudinal conductance $\Delta\sigma_{xx}$ of post-annealed sample as a function of magnetic field at different temperature, $\Delta\sigma_{xx} = \sigma_{xx}(H) - \sigma_{xx}(0)$. The solid lines show the fit of HLN equation. (c) Phase coherence length l_φ of substrate-heated and post-annealed samples as a function of temperature.

It is clear that both l_φ decrease with the temperature increasing from 2 K to 10 K and this monotonous reduction of coherence length was also observed in other topological insulator systems.[25,26] It is well-known that the coherence length l_φ is proportional to $T^{-1/2}$ for the two-dimensional system.[27] Here, the power exponents of the two samples are -0.58 and -0.63 (Fig. 5(c)), slightly differ from $-1/2$, suggesting a contribution of the bulk channel. Anyhow, the long phase coherence length encourages us to take its advance in the quantum transport.

It has been shown in this study that the post-annealing Bi_2Te_3 thin films have lower bulk carrier density than the films grown at high substrate temperatures. We note that the achieved carrier density is also lower than the values of samples grown by MBE,[13,14] PLD,[15,16] and CVD.[17] In previous studies, the bulk charge carriers of Bi_2Te_3 mostly originate from point defects like Te_{Bi} antisite donor defects.[29,30] Thus, we can infer that the number of Te_{Bi} antisite defects in the 280 °C annealed samples is smaller than that in the substrate-heated samples. More detailed annealing processes, such as refining the annealing temperature and annealing time, than those used here would be necessary to find the best condition for further reducing the bulk carrier density of Bi_2Te_3 thin films. Besides, more microstructure characterizations are needed to reveal the relationship between carrier density and the heat treatment process of Bi_2Te_3 thin films.

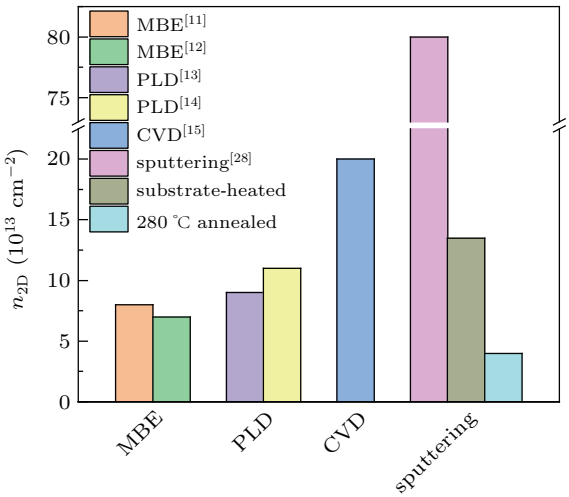


Fig. 6. Comparison of our carrier density of Bi_2Te_3 thin films with previous reported data.

In conclusion, we present a feasible and scalable method based on magnetron sputtering to obtain high-quality Bi_2Te_3 films, which was firstly sputtered at room temperature and then followed with post-annealing. It enables the growth of highly-oriented Bi_2Te_3 thin films with larger grain size and smoother interface. The results of electrical transport show that it has a lower carrier density down to 4.0×10^{13} cm^{-2} as well as a larger coherent length up to 228 nm. The appearance of the WAL effect and EEI in our sample indicates that it keeps the character of the topological surface state. This work fa-

cilitates the fabrication of TI-based devices for electronic and spintronic applications.

References

[1] Xia Y, Qian D, Hsieh D, Wray L, Pal A, Lin H, Bansil A, Grauer D, Hor Y S, Cava R J and Hasan M Z 2009 *Nat. Phys.* **5** 398

[2] Chen Y L, Analytis J G, Chu J H, Liu Z K, Mo S K, Qi X L, Zhang H J, Lu D H, Dai X, Fang Z, Zhang S C, Fisher I R, Hussain Z and Shen Z X 2009 *Science* **325** 178

[3] Hsieh D, Xia Y, D Qian, Wray L, Meier F, Dil J H, Osterwalder J, Patthey L, Fedorov A V, Lin H, Bansil A, Grauer D, Hor Y S, Cava R J and Hasan M Z 2009 *Phys. Rev. Lett.* **103** 146401

[4] Zhang T, Cheng P, Chen X, Jia J F, Ma X, He K, Wang L, Zhang H, Dai X, Fang Z, Xie X and Xue Q K 2009 *Phys. Rev. Lett.* **103** 266803

[5] Chang C Z, Zhang J S, Feng X, Shen J, Zhang Z C, Guo M H, Li K, Ou Y B, Wei P, Wang L L, Ji Z Q, Feng Y, Ji S H, Chen X, Jia J F, Dai X, Fang Z, Zhang S C, He K, Wang Y Y, Lu L, Ma X C and Xue Q K 2013 *Science* **340** 167

[6] He X, Guan T, Wang X, Feng B, Cheng P, Chen L, Li Y and Wu K 2012 *Appl. Phys. Lett.* **101** 123111

[7] Stephen G M, Vail O A, Lu J, Beck W A, Taylor P J and Friedman A L 2020 *Sci. Rep.* **10** 4845

[8] Liu Y H, Chong C W, FanChiang C M, Huang J C, Han H C, Li Z, Qiu H, Li Y C and Liu C P 2017 *ACS Appl Mater Interfaces* **9** 12859

[9] Yuan H T, Liu H W, Shimotani H, Guo H, Chen M W, Xue Q K and Iwasa Y 2011 *Nano Lett.* **11** 2601

[10] Liao J, Ou Y B, Liu H W, He K, Ma X C, Xue Q K and Li Y Q 2017 *Nat. Commun.* **8** 16071

[11] Harrison S E, Li S, Huo Y, Zhou B, Chen Y L and Harris J S 2013 *Appl. Phys. Lett.* **102** 171906

[12] Zhang G, Qin H, Teng J, Guo J, Guo Q, Dai X, Fang Z and Wu K 2009 *Appl. Phys. Lett.* **95** 053114

[13] Wu H, Zhang P, Deng P, Lan Q, Pan Q, Razavi S A, Che X, Huang L, Dai B, Wong K, Han X and Wang K L 2019 *Phys. Rev. Lett.* **123** 207205

[14] Rosenbach D, Oellers N, Jalil A R, Mikulics M, Kölzer J, Zimmermann E, Mussler G, Bunte S, Grützmacher D, Lüth H and Schäpers T 2020 *Adv. Electron. Mater.* **6** 2000205

[15] Liao Z, Brahlek M, Ok J M, Nuckols L, Sharma Y, Lu Q, Zhang Y and Lee H N 2019 *APL Materials* **7** 041101

[16] Zhang S X, McDonald R D, Shekhter A, Bi Z X, Li Y, Jia Q X and Picraux S T 2012 *Appl. Phys. Lett.* **101** 202403

[17] Wang Z H, Yang L, Li X J, Zhao X T, Wang H L, Zhang Z D and Gao X P 2014 *Nano Lett.* **14** 6510

[18] Guo Q, Wu Y, Xu L, Gong Y, Ou Y, Liu Y, Li L, Yan Y, Han G, Wang D, Wang L, Long S, Zhang B, Cao X, Yang S, Wang X, Huang Y, Liu T, Yu G, He K and Teng J 2020 *Chin. Phys. Lett.* **37** 057301

[19] Zhu S, Meng D, Liang G, Shi G, Zhao P, Cheng P, Li Y, Zhai X, Lu Y, Chen L and Wu K 2018 *Nanoscale* **10** 10041

[20] Björck M and Andersson G 2007 *J. Appl. Crystallogr.* **40** 1174

[21] Chen J, He X Y, Wu K H, Ji Z Q, Lu L, Shi J R, Smet J H and Li Y Q 2011 *Phys. Rev. B* **83** 241304

[22] Zhao Y, Chang C Z, Jiang Y, DaSilva A, Sun Y, Wang H, Xing Y, Wang Y, He K, Ma X, Xue Q K and Wang J 2013 *Sci. Rep.* **3** 3060

[23] Wang W J, Gao K H and Li Z Q 2016 *Sci. Rep.* **6** 25291

[24] Hikami S, Larkin A I and Nagaoka Y 1980 *Prog. Theor. Phys.* **63** 707

[25] Takagaki Y, Giussani A, Perumal K, Calarco R and Friedland K J 2012 *Phys. Rev. B* **86** 125137

[26] Assaf B A, Cardinal T, Wei P, Katmis F, Moodera J S and Heiman D 2013 *Appl. Phys. Lett.* **102** 012102

[27] Altshuler B L, Aronov A G and Khmelnitsky D E 1982 *J. Phys. C: Solid State Phys.* **15** 7367

[28] Wang X, He H, Wang N and Miao L 2013 *Appl. Surf. Sci.* **276** 539

[29] Kampmeier J, Borisova S, Plucinski L, Luysberg M, Mussler G and Grützmacher D 2015 *Crystal Growth & Design* **15** 390

[30] Scanlon D O, King P D, Singh R P, de la Torre A, Walker S M, Balakrishnan G, Baumberger F and Catlow C R 2012 *Adv. Mater.* **24** 2154